where ρ is the radius of curvature.

The beam will be taken to be of rectangular cross section with a depth of b and a height of h. The distance from the bottom of the beam to the neutral axis will be taken to be c.

If Eqs. (1–4) are combined, the following relations result for the curvature and the location of the neutral axis:

$$\int_{-c}^{0} \alpha t \frac{y}{\rho(t)}\,dy + \int_{0}^{h-c} \alpha c \frac{y}{\rho(t)}\,dy + \int_{0}^{h-c} \left[E(0) \times \frac{y}{\rho(t)} + \int_{0}^{t} \frac{y}{\rho(t-\tau)} \dot{E}(\tau)d\tau\right] dy = 0 \tag{5}$$

$$\int_{-c}^{0} \alpha t \frac{y^2}{\rho(t)}\,dy + \int_{0}^{h-c} \alpha c \frac{y^2}{\rho(t)}\,dy + \int_{-c}^{h-c} \left[E(0) \times \frac{y^2}{\rho(t)} + \int_{0}^{t} \frac{y^2}{\rho(t-\tau)} \dot{E}(\tau)d\tau\right] = \frac{M(t)}{b}$$

After the spatial integration is carried out, Eqs. (5) become

$$\frac{c^2(t)}{\rho(t)}[\alpha c - \alpha t] + \left[\frac{\alpha c}{\rho(t)} + \frac{E(0)}{\rho(t)} + \int_{0}^{t} \frac{\dot{E}(\tau)}{\rho(t-\tau)}\,d\tau\right][h - 2hc(t)] = 0 \tag{6}$$

$$\frac{c^3(t)}{\rho(t)}[\alpha c - \alpha t] + \left[\frac{\alpha c}{\rho(t)} + \frac{E(0)}{\rho(t)} + \int_{0}^{t} \frac{\dot{E}(\tau)}{\rho(t-\tau)}\,d\tau\right][h^3 - 3h^2c(t) + 3hc^2(t)] = 3M(t)$$

After Eqs. (6) are solved for $c(t)$ and $\rho(t)$, Eqs. (1, 2, and 4) can be used to obtain the stresses.

If the beam is subjected to a constant radius of curvature, $\rho(t) = k$, Eqs. (6) can be solved analytically for $c(t)$ and $M(t)$. Figure 1 shows the stresses resulting from such a deformation for the cases $\alpha c \neq \alpha t$ and $\alpha c = \alpha t$. These results are not very interesting since the stresses obtained from the former are less than the latter. Thus if a design is based on the simpler analysis of assuming $\alpha c = \alpha t$, the results would be safe.

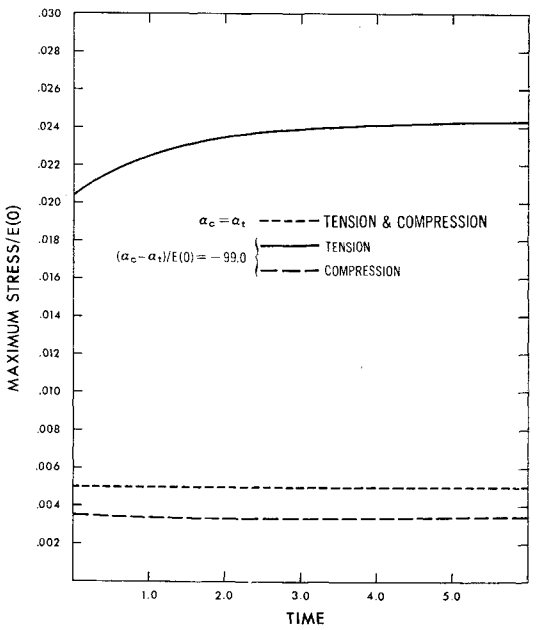

Fig. 3 Maximum stress vs time; $M/E(0) = 0.001$, $(\alpha_c - \alpha_t)/E(0) = -99.0$.

If, however, a constant moment is applied at $t = 0$, Eqs. (6) become harder to solve. To effect a solution for this case, the equations were finite-differenced and a Newton-Raphson scheme was used to solve them numerically. Figures 2 and 3 show the maximum stress in this case for two values of the parameters $(\alpha c - \alpha t)/E(0)$. Notice that in both cases, the maximum stress that is predicted by using $\alpha c = \alpha t$ is over 50% less than that predicted by the analysis when $\alpha c \neq \alpha t$.

In all figures, the following numerical values were used for the parameters:

$$b = 1,\ h = 1,\ \frac{E(t)}{E(0)} = 1 + e^{-t/\beta},\ \frac{M(t)}{E(0)} = 0.001$$

Conclusion

Although the results presented are for the simplest case that could be considered, there appear to be several safe generalizations one can make. The first is that the greater the difference in αt and αc, the more the actual stress will depart from that predicted by assuming that $\alpha c = \alpha t$. Also, for a given difference, the smaller $E(0)$, the greater the difference in stress for $\alpha c = \alpha t$ and $\alpha c \neq \alpha t$. Thus for materials with a relatively strong matrix, the error involved in using a standard analysis would not be too great. However, for materials with a weak matrix, a design based on the standard analysis could be grossly in error.

Computation of Axisymmetric Contractions

HARTMUT H. BOSSEL*
University of California, Santa Barbara, Calif.

Introduction

CONTRACTIONS, as in wind tunnels, must fulfill two basic requirements. First, the exit velocity at the narrow end must be uniform and parallel. Second, there must be no regions of separation caused by adverse pressure gradients at the wall which may appear at the start of the contraction and at the neck.

Many wind-tunnel contractions have been, and are being, designed by intuition. Unless model tests are made, the results are unpredictable and often unsatisfactory. It is clearly better to base the design on theoretical studies. Several methods for the design of axisymmetric contractions have been proposed over the years, unfortunately, all without experimental verification. In reviewing these methods for possible application to the design of a low-turbulence wind-tunnel contraction, it was found that none was entirely satisfactory. The method to be presented here is an outgrowth of these studies. It is a reformulation of Thwaites' solution[1] and has been found to be quick and convenient. An axisymmetric contraction with a 16/1 contraction ratio was designed using this method, built, and tested. The measured velocity distributions at entrance, exit, and on the wall will be presented and compared with the theoretical data.

Methods for the computation of axisymmetric potential flow fall into four broad categories: 1) adaptation of two-di-

Received January 13, 1969; revision received May 20, 1969. The author gratefully acknowledges the assistance of mechanical engineering students W. Sun, who built the contraction, L. Fafarman, who assembled the wind tunnel, and J. D. Riley, who carried out the measurements.

* Assistant Professor of Mechanical Engineering. Member AIAA.

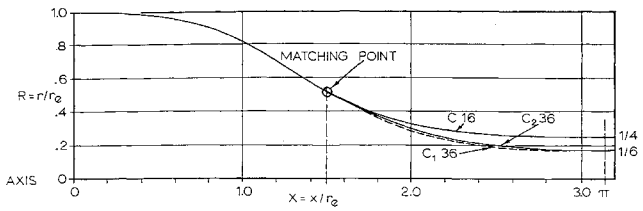

Fig. 1 Contraction contours.

mensional results, 2) distributed singularities, 3) relaxation, 4) and separation of variables. Of these, only series solution based on separation of variables offers high accuracy and flexibility for a small computing effort.

Separation of Variables

Using entrance radius r_e and entrance velocity u_0 as reference quantities, we introduce nondimensional variables for convenience

$$X = x/r_e, \quad U = u/u_0 = (1/R)\partial\Psi/\partial R$$
$$R = r/r_e, \quad V = v/u_0 = (-1/R)\partial\Psi/\partial R$$

The equation for Stokes' stream function of inviscid axisymmetric flow is

$$\frac{\partial^2\Psi}{\partial X^2} - \frac{1}{R}\frac{\partial\Psi}{\partial R} + \frac{\partial^2\Psi}{\partial R^2} = 0$$

Assuming $\Psi(R,X) = F(R)G(X)$, the equation separates into two ordinary differential equations for $F(R)$ and $G(X)$. Depending on the choice of separation constant, we obtain different types of solutions (see Lamb[2]). Applying the boundary condition that velocities must be finite on the axis and using the linearity property, three possible series solutions may be constructed:

$$\Psi_a(R,X) = \frac{R^2}{2} + \sum_{n=2}^{\infty} R^{2n} G_n(X) = \frac{1}{2}\sum_{n=1}^{\infty} \frac{(-1)^{n-1}U_{ax}^{(2n-2)}(X)R^{2n}}{2^{2n-2}n[(n-1)!]^2}$$

$$\Psi_b(R,X) = \frac{R^2}{2} + R\sum_{n=1}^{\infty} \times J_1(\mu_n R)[a_n \exp(\mu_n X) + b_n \exp(-\mu_n X)]$$

$$\Psi_c(R,X) = \frac{R^2}{2} + R\sum_{n=1}^{\infty} I_1(\mu_n R)[c_n \sin(\mu_n X) + d_n \cos(\mu_n X)]$$

The J_n are the ordinary and the I_n the modified Bessel functions. $U_{ax}(X)$ is the velocity distribution on the axis. Solution Ψ_a was used by Szczeniowski,[3] and Tsien,[4] and Cohen and Ritchie,[5] and solution Ψ_c has been applied by Thwaites.[1] These authors either prescribe the velocity distribution on the axis,[3-5] or put some constraints of uniformity and parallelism on the entrance velocity distribution.[1]

Solution Ψ_a is restricted to families of velocity distributions on the axis which permit analytic expression of their derivatives. The velocities at entrance and exit (a finite distance apart) are neither uniform nor parallel, and a rather long contraction is required to avoid a strong adverse pressure gradient at the entrance. Solution Ψ_b is aperiodic. The velocity distribution on the axis must be expressed in a series of sinh and cosh terms.

Solution Ψ_c is periodic in the axial direction. The velocity on the axis can easily be expressed as a Fourier series. The assumption $c_n = 0$ results in parallel flow at entrance and exit, but the velocity distribution at these stations is necessarily nonuniform. A uniform velocity distribution ($d_n = 0$) could be achieved at the cost of nonparallel flow at entrance and exit. The fact that the entrance and exit velocity distributions in a contraction cannot be both uniform and parallel if entrance and exit are a finite distance apart is a basic result of potential theory and not of the particular solutions used.

The present method uses solution Ψ_c, but prescribes the wall contour. Herein lies an important difference between previous methods and the present approach. Local changes in the wall contour have mainly local effects on the flow near the wall, whereas changes in the velocity distribution on the axis affect the whole flowfield. Thus, a trial-and-error procedure prescribing the wall contour is rapidly converging. Two or three corrections applied to an initial assumption for the wall contour will generally yield a contraction free of adverse pressure gradients and with an acceptable exit velocity profile.

Application of Solution Ψ_c and Theoretical Results

The periodic solution for parallel inflow and outflow becomes

$$\Psi_c(R,X) = a_0\frac{R^2}{2} + \sum_{n=1}^{\infty}\frac{a_n}{n} RI_1(nR)\cos nX \qquad (1)$$

The wall streamline must satisfy the equation

$$\Psi_c = \text{const} = \Psi_w$$

If the series is truncated after N terms and if the wall contour R_i is prescribed at N points X_i, we obtain a system of N equations for the unknown Fourier coefficients a_n

$$\sum_{n=1}^{N}\frac{a_n}{n} R_i I_1(nR_i)\cos nX_i = \Psi_w - a_0\frac{R_i^2}{2};\ i = 1,2,\ldots,N \qquad (2)$$

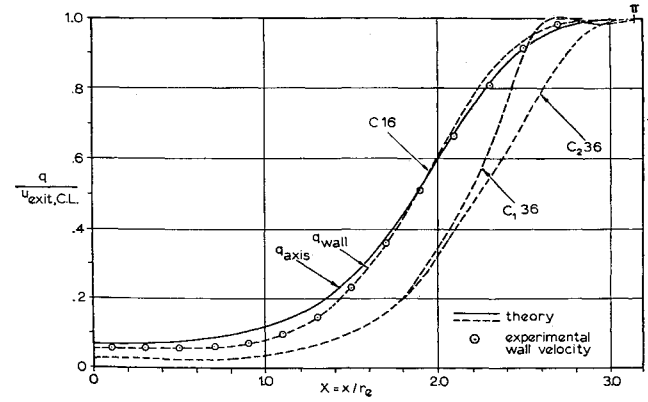

Fig. 2 Theoretical velocity distributions for the 16/1 (C 16) and 36/1 (C 36) contractions, and experimental wall velocity for the 16/1 contraction. $C_1$36, original contour; $C_2$36, modified contour.

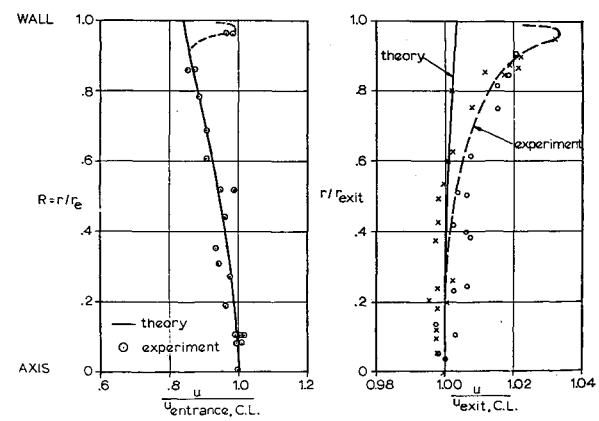

Fig. 3 Theoretical and experimental velocity distributions at entrance and exit of the 16/1 contraction. Crosses and circles symbolize points on opposite sides of the axis.

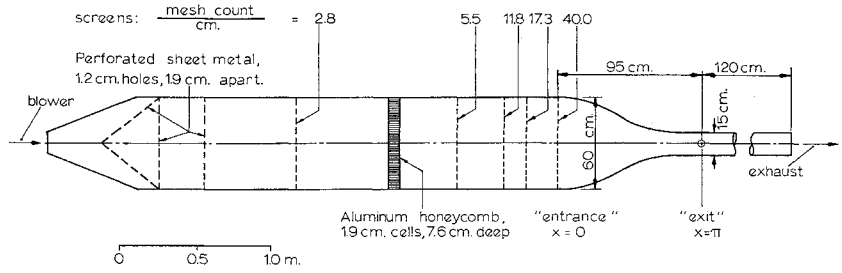

Fig. 4 Wind tunnel for the testing of the 16/1 contraction.

Once the a_n are known, stream function and velocities follow in the entire flowfield.

The method was used in the following manner: A scale drawing was made of the contraction for which the flow was to be computed. Coordinates were read off to three decimal places at selected points, usually 15 to 20. It was found to be advantageous to space the points more closely near the entrance, and farther apart near the exit. The coordinates were supplied to a computer program which generated the 15 to 20 equations (2) and determined an equal number of coefficients a_n of the series solution (1). Stream function and velocity magnitude at approximately 700 points in the contraction flowfield were then computed. The total computation using 19 Fourier coefficients takes about 10 sec on an IBM 360/65 computer. The wall velocities follow by interpolation for gridpoints next to the wall. The wall contour was changed where adverse velocity gradients were found.

Figs. 1–3 present the results of such calculations for contraction ratios of 16/1 and 36/1 and a length ratio of $L/D = \pi/2$. To investigate the feasibility of interchangeable exit sections, the basic 16/1 contraction was modified beginning at $X = 1.5$. The first modification ($C_1 36$) showed an adverse pressure gradient near the neck (Fig. 2). The contour was changed ($C_2 36$) and the adverse pressure gradient disappeared. It should be noted that the difference between contours $C_1 36$ and $C_2 36$ is minor, whereas the effect on the wall velocity distribution is pronounced. The result underscores what was said earlier about the unpredictability of design by intuition. Note that the effects of periodicity can be diminished by prescribing, for purposes of computation only, nearly parallel extensions at both ends of the contraction.

To investigate the effects of periodicity, the flowfield corresponding to Tsien's velocity distribution[4] and a contraction ratio of 16/1 was computed both by using the aperiodic solution Ψ_a and the periodic solution Ψ_c. In the latter case Tsien's velocity distribution was inverted and repeated at $X = \pm\pi$. The differences over the whole flowfield were minor and had to be partly attributed to series truncation and poor convergence of Tsien's solution for larger R.

Experimental Results

The 16/1 contraction of Fig. 1 was built in fiberglass-resin construction over an axisymmetric wooden mold. It has an exceptionally smooth surface. Its dimensions and those of the wind tunnel in which it was installed are given in Fig. 4. The open area ratio of all screens was greater than 57% in order to avoid the jet coalescence problem discussed by Bradshaw.[6] The turbulence level in the tunnel was less than 0.25%. Tuft observations indicated that the flow at entrance and exit was parallel to about ±1°. All tests were made at a Reynolds number $ud/\nu = 628{,}000$ based on the exit diameter and velocity.

The velocity pressures at the entrance and exit cross sections were obtained from pitot tube traverses. Experimental results for the wall velocity are plotted in Fig. 2 together with the theoretical curve for the (inviscid) contraction contour. This contour corresponds to the test contraction; manufacturing errors and boundary-layer effects at the test Reynolds number were taken into account. The boundary-layer displacement thickness was computed using the method of Thwaites[7] appropriately modified for axisymmetric flow following Rott and Crabtree.[8]

The experimental and theoretical values for the wall velocity (Fig. 2) are seen to agree very closely in the low-velocity part of the contraction up to where $q/u_{exit} = 0.6$ approximately. The two distributions deviate by a maximum of about 4% in the high-velocity part of the contraction. In this part the experimental wall velocity distribution agrees more closely with the theoretical velocity distribution on the axis. The theoretical wall velocity distribution is conservative with respect to adverse pressure gradients in the neck.

The discrepancy between experimental and theoretical wall velocity in the neck can be explained by considering, qualitatively, both the periodic and the aperiodic contraction generated by source and sink rings, and source rings, respectively. An additional positive wall velocity component appears as a contribution of the downstream sink ring in the periodic case. The corresponding analytical solution thus overestimates the wall velocity at the neck somewhat if applied to the aperiodic case.

The experimental values for the velocity distribution at the entrance (Fig. 3) follow the theoretical prediction over the whole region with the exception of the outer 5% of the radius. The local velocity increase there is the result of a very short 5° convergence required to overcome a 1% diameter mismatch between tunnel and contraction. The velocity increase should, therefore, not be expected in other applications.

The theoretical solution predicts a maximum deviation of the exit velocity from the centerline velocity of 0.3% (Fig. 3). The experimental results show a deviation of about 1% at 80% of the radius, and about 3% at 95% of the radius, before the velocity falls again off to zero through the boundary layer. The discrepancy in the two velocity distributions clearly is of an inviscid nature and must be attributed to the fact that the theoretical result is based on a periodic solution, whereas the experimental result corresponds to an aperiodic situation. The same experimental velocity distribution was also obtained with the test section removed and the flow exhausting into ambient air through a sharp-lipped parallel exit 2.5 cm downstream from the exit velocity measuring station.

On the basis of these results, it is felt that the present method of computation can be used with some confidence in the design of arbitrary contractions, even at high contraction ratios and short lengths. The application of the method is simple and convenient and the computation extremely rapid.

References

[1] Thwaites, B., "On the Design of Contractions for Wind Tunnels," R&M 2278, March 1946, British Aeronautical Research Council.

[2] Lamb, H., *Hydrodynamics*, 6th ed., Dover, New York, 1945 (Reprint), pp. 134–139.

[3] Szczeniowski, B., "Contraction Cone for a Wind Tunnel," *Journal of the Aeronautical Sciences*, Vol. 10, No. 8, Oct. 1943, pp. 311–312.

[4] Tsien, H. S., "On the Design of the Contraction Cone for a Wind Tunnel," *Journal of the Aeronautical Sciences*, Vol. 10, No. 2, Feb. 1943, pp. 68–70.

[5] Cohen, J. J. and Ritchie, N. J. B., "Low-Speed Three Dimensional Contraction Design," *Journal of the Royal Aeronautical Society*, Vol. 66, 1962, pp. 231–236.

[6] Bradshaw, P., "The Effect of Wind Tunnel Screens on 'Two-dimensional' Boundary Layers," Rept. 1085, 1963, National Physical Lab., Great Britain.

[7] Thwaites, B., "Approximate Calculation of the Laminar Boundary Layer," *Aeronautical Quarterly*, Vol. 1, 1949, pp. 245–80.

[8] Rott, N. and Crabtree, L. F., "Simplified Laminar Boundary Layer Calculations for Bodies of Revolution and for Yawed Wings," *Journal of the Aeronautical Sciences*, Vol. 19, No. 8, Aug. 1952, pp. 553–565.

Determination of Charge/Mass and Thrust from a Positively Charged Colloidal Beam

BRIAN MAKIN* AND ALFRED WILLIAM BRIGHT†
The University of Southampton, Southampton, England

1. Introduction

THE determination of the average charge/mass (q/m) of an aerosol or a charged colloidal beam at atmospheric pressure is an important parameter in any optimization study. A method is proposed which can be used for q/m measurements in either vacuum or at atmospheric pressure using standard laboratory equipment. The technique may prove to be useful in the performance analysis of some applications which use an electrically charged colloidal beam as the working medium.

A commercial process that has proved to be efficient and successful[1] is the process of electrastatic painting. A second field of interest is the electric propulsion of spacecraft. A charged colloidal beam with a relatively high charge/mass on each droplet (approximately 10^4 C/kg) is a serious contender for the present types of electric propulsion devices employing mercury, cesium, or potassium.[2] A singly charged cesium ion has a charge/mass of 7.26×10^5 coul/kg. A third more recent application in which charged aerosols could be important is in the generation of electricity (EGD).[3]

In all these applications the most important parameter which limits the efficiency is the ratio of charge/mass of each charged droplet. Many papers have been written on the dynamics of charged particles.[4,5] In the case of colloidal propulsion it is necessary to consider chemistry of the liquid during the formation of the droplet. This is a complex problem of charge neutralisation of the liquid ions at the wall of the nozzle or capillary needle. A survey of this problem has been given by Wineland and Hunter predicting criteria for stable operation.[6]

In this Note a method is put forward for determining the average charge/mass ratio for a charged aerosol which can be used at atmospheric pressure for any solvent, and in vacuo for liquids with a low vapour pressure where evaporation from a free surface is negligible. From a few parameters which can be measured accurately with standard equipment (chemical balance, oscilloscope, high-voltage generator), it is possible to determine the liquid thrust, the total thrust (liquid thrust plus liquid corona thrust), efficiency, and average exhaust velocity.

2. Experimental Arrangement and Theory

An aerosol generator was constructed from a glass tube of 5-mm o.d. with a glass nozzle of 0.45-mm-diam bore. Two similar tubes were fixed to a Teflon cup that was located on a low-friction pivot mounted vertically. The glass nozzles were positioned at right angles to the glass tubes and the assembly could rotate freely. The length of the radius arm was 12 cm. In these tests one nozzle was permanently sealed to eliminate any possible differences in efficiency of operation between the nozzles.

The Teflon cup was filled with liquid and an electrode was positioned below the liquid surface. When a high voltage was applied to the electrode, an aerosol was generated from the open nozzle. At atmospheric pressure the rotor revolved at speeds up to 12 rad/sec, with a wide range of liquids. Power was supplied from a 60 kv, 200 μa Brandenburg generator. The angular velocity and acceleration were measured by arranging the rotor to intersect a light beam. The equipment was located in a vacuum chamber and experiments were carried out at atmospheric pressure and subsequently at the ultimate 10^{-3} torr vacuum of the system. At atmospheric pressure the dominant process is expected to be the corona effect or electric wind. In vacuo the corona thrust would be minimized and hence any thrust developed would be produced from the charged colloidal beam.

In general, we can assume the thrust developed by the rotor consists of corona thrust (T_C), and from the acceleration of the charged colloid beam or liquid thrust (T_L).

In dynamic equilibrium

$$T_L + T_C = \mathrm{VI}\eta/\mathrm{r}\dot{\theta} \tag{1}$$

where VI is the input power, r the radius arm, $\dot{\theta}$ the equilibrium angular velocity, and η the efficiency.

The general equation of motion is

$$(T_L + T_C)\,\mathrm{r} - \mathrm{F} = J\ddot{\theta} \tag{2}$$

where F is the frictional couple of the pivot and J the moment of inertia of the rotor about a vertical axis through the electrode. At equilibrium $\ddot{\theta} = 0$ and F is determined at the equilibrium velocity $\dot{\theta}$ from a run down experiment.

A particle of charge q accelerating through a potential V volts will reach a terminal velocity v given by $V_q = \frac{1}{2}\,mv^2$. The thrust developed by the droplet (T_L) is equal to the rate of change of momentum; hence $T_L = \dot{m}v$, where $\dot{m}$ is the mass flow rate of the liquid. Hence the average charge/mass ratio $\langle q/m \rangle$ per droplet is

$$\langle \mathrm{q/m} \rangle = T_L^2/2\mathrm{V}\dot{m}^2 \tag{3}$$

Also, the power developed in accelerating the droplet is equal to the average work done ($\frac{1}{2}\,T_L v$). If we assume the efficiency

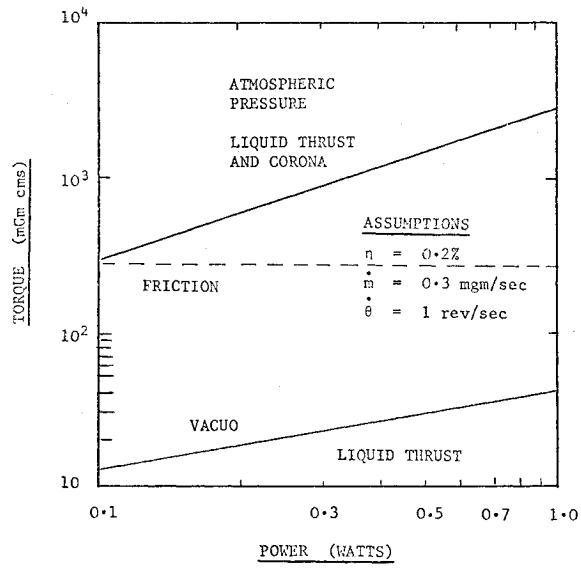

Fig. 1 Theoretical variation of torque with power.

Received December 16, 1968; revision received June 27, 1969.

* Lecturer, Department of Electrical Engineering.
† Reader, Department of Electrical Engineering.